Calcification response of reef corals to seasonal upwelling in the northern Arabian Sea (Masirah Island, Oman)

Philipp M. Spreter[1], Markus Reuter[2], Regina Mertz-Kraus[3], Oliver Taylor[4], Thomas C. Brachert[1]

[1]Institut für Geophysik und Geologie, Universität Leipzig, Talstraße 35, 04103 Leipzig, Germany
[2]Institut für Geographie und Geologie, Universität Greifswald, Friedrich-Ludwig-Jahn-Str. 17a, 17489 Greifswald, Germany
[3]Institut für Geowissenschaften, Johannes Gutenberg-Universität Mainz, Johann-Joachim-Becher-Weg 21, 55128 Mainz, Germany
[4]Five Oceans Environmental Services, Villa 1756, Way 3021; Shatti Al Qurm, Muscat, Sultanate of Oman

Correspondence to: Philipp M. Spreter (philipp.spreter@uni-leipzig.de)

Tropical shallow-water reefs are the most diverse ecosystem in the ocean. Its persistence rests upon adequate calcification rates of the reef building biota, such as reef corals. The calcification mechanism of reef corals performs best in oligotrophic environments with high seawater saturation states of aragonite (Ω_{sw}), leading to an increased vulnerability to anthropogenic ocean acidification and eutrophication. The calcification response of reef corals on rapid changes in Ω_{sw} and seawater nutrient concentrations is currently under discussion in coral science. Here we present *Porites* calcification records from the northern Arabian Sea upwelling zone and investigate the coral calcification response to low Ω_{sw} and high nutrient concentrations due to seasonal upwelling. Calcification rate was determined from the product of skeletal extension and bulk density. Skeletal Ba/Ca and Li/Mg proxy data allowed to identify skeletal portions calcified during upwelling and non-upwelling seasons, respectively, and to reconstruct growth temperatures. With regard to sub-annual calcification patterns, our results demonstrate compromised calcification rate during the upwelling season. This is due to declining extension rate, which we attribute to light dimming caused by high primary production. Interestingly, skeletal density shows no relationship with temporally low Ω_{sw} during upwelling. This suggests relatively constant, year-round saturation states of aragonite at the site of calcification (Ω_{cf}) independent of external variability of Ω_{sw}. Although upwelling does not affect seasonal density variability, exceptionally low mean annual density implies permanent Ω_{cf} adjustment to the lowest sub-annual Ω_{sw} (e.g., upwelling). In the Arabian Sea upwelling zone, mean annual calcification rate is similar to *Porites* from non-upwelling regions because low skeletal density is compensated by high extension growth. We anticipate maintenance of adequate reef coral calcification rate under global change is largely reliant on extension rate, whose variable responses to nutrients either compensate or exacerbate negative effects of diminished skeletal density associated with ocean acidification.

1 Introduction

Tropical coral reefs are the most diverse aquatic ecosystem on the planet (Hughes et al., 2017). Their basic building blocks are the calcareous (aragonite) skeletons of symbiotic scleractinian corals (reef corals) and sustained precipitation of skeletal carbonate (calcification) is fundamental for maintaining their structure and function (Perry et al., 2012). Optimum calcification of reef corals is found in oligotrophic water masses of temperatures between 21 °C to 29.5 °C and a saturation state of seawater with respect to aragonite >3.3 (Ω_{sw}) (Kleypas et al., 1999). Anthropogenic greenhouse gas emissions threaten reef coral calcification by increasing sea surface temperature (SST) and by causing ocean acidification. In addition, land use, discharge of wastewater and fish farming turn the near-shore shallow-marine environments towards more eutrophic conditions. The responses of reef coral calcification to~~on~~ the rapidly changing environment are highly variable and remain ~~contemporarily~~ a matter of intense research (Cornwall et al., 2021; Guan et al., 2020; Hall et al., 2018).

Coral calcification rate (g cm^{-2} yr^{-1}) is the product of linear extension rate (cm yr^{-1}) measured along the axis of maximum growth and bulk density (g cm^{-3}) (Dodge and Brass, 1984). Linear extension rate in reef corals is linked to efficiency of photosynthesis in symbiotic micro-algae, providing energy to the host for upward growth of the skeleton (Muscatin et al., 1981; Sun et al., 2008). Availability of light and water temperature are the main drivers controlling photosynthetic efficiency and thus positively related to the extension rate (Al-Rousan, 2012; Logan and Tomascik, 1991; Lough and Barnes, 2000). At certain taxon-specific threshold temperatures, however, extension rate declines rapidly due to thermal stress for the micro-algae symbionts (Cantin et al., 2010). Due to sub-annual variations in extension rate, skeletal portions of high and low density are formed, with high-density bands (HDBs) coinciding with low extension rate (and vice versa for low-density bands = LDBs) (DeCarlo and Cohen, 2017; Highsmith, 1979; Klein and Loya, 1991; Knutson et al., 1972). In addition, aragonite saturation of the calcifying fluid (Ω_{cf}) determines bulk skeletal density (Mollica et al., 2018). Ω_{cf} is approximately five times higher than the aragonite saturation of the external seawater (Ω_{sw}) and long-term changes in Ω_{sw} due to ocean acidification lead to declining Ω_{cf} (McCulloch et al., 2017; D'Olivo et al., 2019). Intra-annually, corals are, however, able to maintain relatively stable levels of Ω_{cf} largely independent of short term variations in Ω_{sw} by upregulating their internal pH_{cf} and DIC_{cf} pool (McCulloch et al., 2017; DeCarlo et al., 2018; D'Olivo and McCulloch, 2017, Ross et al., 2019a).

Near-shore coral reefs are increasingly exposed to anthropogenic eutrophication induced by land use, fish farming and sewage disposal (Lapointe and Clark, 1992; Chen et al., 2019; Chen and Yu, 2011). Eutrophication can have both beneficial as well as detrimental effects on coral growth, depending on the kind of available nutrients and their concentration~~, however~~ (Tomascik and Sander, 1985; Tomascik, 1990). In general, reef corals are highly adapted to oligotrophic waters with micro-algae symbionts to allow an efficient use of essential nutrients (Muscatine and Porter, 1977). This enables ~~and to~~ outcompeting~~e~~ other fast-growing biota on a reef whose growth is inhibited by the undersupply of nutrients (Vermeij et al., 2010; Barott and Rohwer, 2012). Strong eutrophication disturbs this adaptive advantage, leading to harmful algal blooms followed by reef coral mass mortality (Al Shehhi et al., 2014) and reef destruction due to the increasing abundance of bioeroders (Hallock, 1988). However, moderate increases of certain nutrients such as ortho-phosphate (PO_4^{3-}) have been shown to promote linear extension

rate (Bucher and Harrison, 2001; Dunn et al., 2012; Koop et al., 2001). The opposite effect is reported for nitrate (NO_3^-), even though the calcification response is less pronounced compared to PO_4^{3-} (Koop et al., 2001). In general, increasing eutrophy is considered to cause reef corals to sacrifice skeletal density for increased extension rate ("stretching modulation of skeletal growth"), which can either lead to enhanced, constant or reduced rates of calcification Increasing eutrophy is considered to explain increasing coral calcification rate along an offshore – inshore gradient where the effect of temperature is negligible (Carricart-Ganivet and Merino, 2001; Carricart-Ganivet, 2004; D'Olivo et al., 2013; Manzello et al., 2015).

Understanding how coral calcification responds to rapid changes in seawater nutrient conditions and Ω_{sw} is critical for more accurate predictions on the persistence of reef habitats under the influence of global change. Tropical upwelling areas are well suited for this kind of research as the upwelling deep water masses are rich in nutrients and low in Ω_{sw}. This allows these regions to serve as natural laboratories to investigate the calcification response of reef corals to these multiple environmental stressors that are likely to affect global coral reefs in the near future (Camp et al., 2018; Wizemann et al., 2018). Published calcification data of the major reef-building coral *Porites* spp. growing within regions affected by seasonal upwelling are generally sparse and only available from three Pacific reef sites (Manzello et al., 2014; Mollica et al., 2018).

In this study, we report the first calcification data (calcification rate, extension rate, skeletal bulk density) of six *Porites* coral specimens from the so far unexplored region of the northern Arabian Sea upwelling zone (Masirah Island, Oman). Three out of the six samples that were considered representative for the site under study were selected for further geochemical analysis (Li/Mg, Ba/Ca). This facilitated the establishment of a detailed sub-annual chronology yielding monthly resolved records of calcification. This approach allowed us for an unprecedented comparison of sub-annual calcification performance between the upwelling and non-upwelling season. In this way, this study improves the general knowledge on seasonal and annual patterns of reef coral calcification under exposure to variable Ω_{sw} and nutrient concentrations, thereby contributes to more accurate predictions on the persistence of reef habitats under the influence of global change.

2 Material and methods

2.1 Arabian Sea climate and oceanography

The Arabian Sea is the northwestern part of the Indian Ocean between India and the Arabian Peninsula (Fig. 1). The regional climate of the Arabian Sea is characterised by a semi-annual alternation of the prevailing wind directions (Beal et al., 2013). During northern hemisphere summer, strong winds of the southwest monsoon (SWM) cross the Arabian Sea in the direction of the low pressure system above the Tibetan Plateau (Findlater, 1969). During winter, reversal of the atmospheric pressure system causes the northeast monsoon (NEM) (Hastenrath and Greischar, 1991). Low wind speeds without preferred orientation typically occur during the two intermonsoon seasons (spring intermonsoon, = SIM; autumn intermonsoon = AIM) (Beal et al., 2013; Lee et al., 2000). Surface wind fields are the driving force behind the upper hydrospheric structure and the seasonal

variation of the oceanic surface current system (Swallow and Bruce, 1966). During summer, southwest monsoonal winds cause a strong coastal current (Oman Coastal Current), which runs northward parallel to the coast of the Arabian Peninsula and

95 induces rigorous upwelling (Currie et al., 1973; Currie, 1992, Smith and Bottero, 1977). Increased nutrient supply during southwest monsoonal upwelling is associated with an increased primary productivity in the euphotic zone (Anderson et al., 1992; Bauer et al., 1991; Quinn and Johnson, 1996) (Fig. 2). Compared to equatorial upwelling regions of the eastern Pacific, the northern Arabian Sea upwelling is characterized by a high phosphate to nitrate ratio (Kleypas et al., 1999). But although nutrient supply is linked to upwelling, concentrations of PO_4^{3-} and NO_3^- remain on a high level throughout the year, because

100 of a prevailing iron limitation of the primary production (Mother Earths Iron Experiment) (Smith, 2001). Southwest monsoonal upwelling furthermore causes a drop in surface water pH, causing seawater aragonite saturation (Ω_{sw}) to decrease temporally from 3.5 – 4 during non-upwelling season to 3 during the upwelling season, which is well below critical values assumed to be required for coral growth (i.e., Ω_{sw} >3.3) (Kleypas et al., 1999; Omer, 2010; Takahashi et al., 2014) (Fig.2).
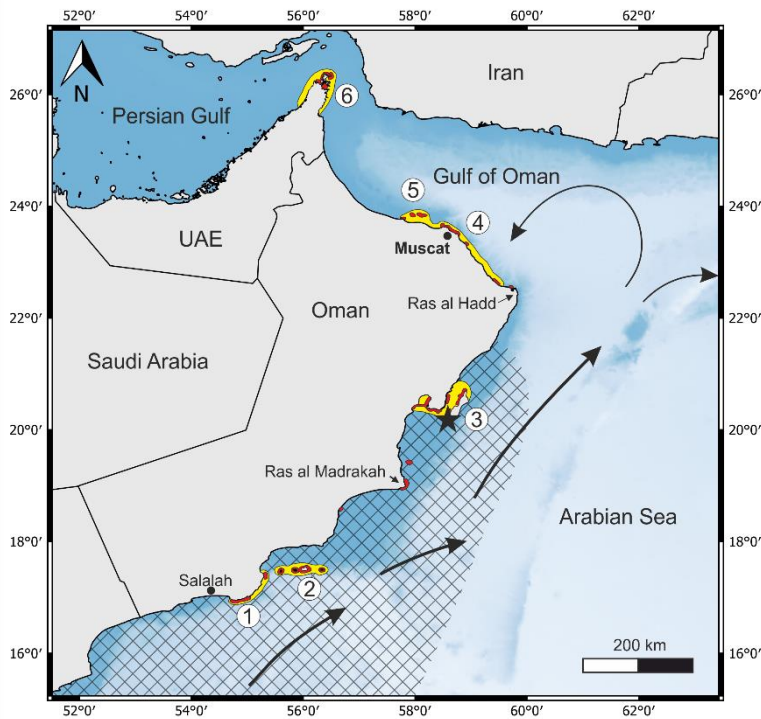
105 **Figure 1: General map of the eastern Arabian Peninsula and the adjacent seas showing the reef sites (red) and coral reef provinces off Oman (yellow) [(1) Marbat, (2) Kuria Muria Islands, (3) Masirah Island and Barr al Hikman, (4) Capital Area (5) Daymaniyat Islands and (6) Musandam (Salm, 1993; Burt et al., 2016)]. The black asterisk marks the sampling site at the southern tip of Masirah Island. Black arrows indicate the Omani current during the southwest monsoon. The hatched area delimitates the region of maximum upwelling inferred from August sea surface temperatures <25 °C (1995-2005 monthly averages; WOA18, Locarnini et**
110 **al., 2018). The blue shading displays water depth gradients (dark blue = shallow, light blue = deep).**
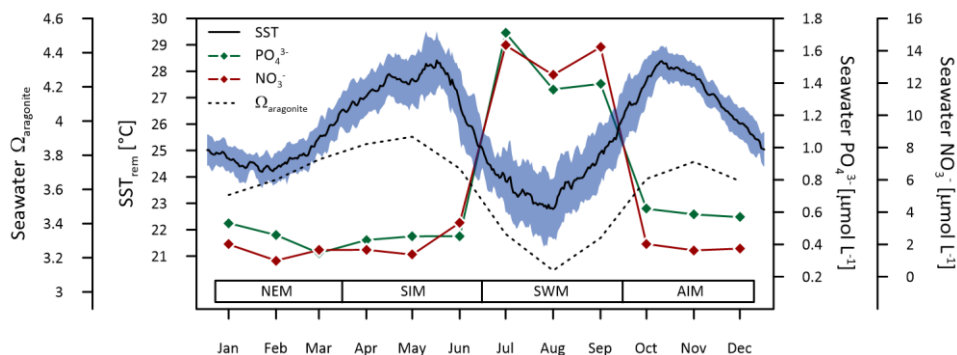
Figure 2: Ocean climatological data estimated from daily SSTs (JPL MUR), monthly seawater phosphate (PO$_4^{3-}$) and nitrate (NO$_3^-$) concentrations (WOA18) (Garcia et al., 2019) and aragonite saturation state ($\Omega_{aragonite}$) (Takahashi et al., 2014) at the sampling site. The blue shaded area represents the deviation (1σ) from averages of daily SSTs within the period 2003-2018. Seasonal abbreviations: NEM (northeast monsoon), SIM (spring intermonsoon), SWM (southwest monsoon), AIM (autumn intermonsoon).

2.2 Coral growth and sample collection at Masirah Island

Coral growth off Oman occurs within six distinct provinces, including Marbat, the Kuria Muria Islands, Masirah Island and Barr al Hikman, the Capital Area, the Daymaniyat Islands and Musandam (Fig. 1; Burt et al., 2016; Salm et al., 1993). The occurrence of corals at Masirah Island is limited to very shallow water depths of 1-4 metres (Glynn, 1993). Fast growing cabbage and brain corals such as *Montipora* and *Platygyra* are the dominant genera, but massive *Porites* are also present (Coles, 1996).

In March 2018, dead coral material from six massive *Porites* colonies (Sample identifier: 5.9; 5.10; 5.13; 5.15; 5.21; 5.22) was collected at the southernmost tip of Masirah Island from the uppermost part of the shore (20.16N, 58.64E) (Fig. 1). This coral occurrence represents a storm deposit related to cyclone Gonu in 2007 (Fritz et al., 2010).

2.3 Methodology

Coral samples were cut to slices of 6 mm thickness parallel to the axis of maximum growth using a rock saw at lowest rotation~~tournament~~ speed and equipped with a water-cooled diamond blade. Subsequent usage of a CNC mill ensured co-planarity with maximum deviations of 1-3 % over the entire slab. The slabs were ultrasonically cleaned in deionized water and dried at 40 °C. Coral slabs were X-rayed using a digital X-ray cabinet (SHR 50 V) to document alternating growth bands of high (HDB) and low density (LDB) (Knutson et al., 1972), biogenic borings, encrustations, and cementation. Sampling transects for all further analyses were carefully selected so as not to be affected by bioerosion and encrustations but normal to HDBs and LDBs following trajectories of maximum linear extension (for the positioning of individual sampling transects see supplementary material, Fig. S1). Density measurements were performed using X-ray densitometry based on CoralXDS software (Helmle et al., 2002, 2011). Grey-scale - density calibrations were verified by measurements of standards for zero density (air, $\rho = 0$ g/cm^{-3}) and massive aragonite (*Tridacna* shell, $\rho = 2.93$ g/cm^{-3}) having the same thickness as the coral slabs.

Maximum target deviations were 0.02 ± 0.01 g cm^{-3} for zero density (air) and 0.03 ± 0.06 g cm^{-3} for massive aragonite (Tridacna shell). Width of density measurement transects were set to 4 mm, including a representative mixture of

140 approximately 12 corallites (4 x 6 mm). Annual extension rate was estimated from the distance between two HDBs of maximum grey scale intensity on the radiographs. The mean annual skeletal density was calculated from the mean of all individual measurements along the transect and within one annual growth increment.

Corals 5.10, 5.13 and 5.21 were selected for Li/Mg and Ba/Ca geochemical analysis based on optimal orientation and traceability of the corallites adjacent to the density measurement transects ~~Adjacent to the density measurement transects of~~

145 ~~coral 5.10, 5.13 and 5.21, skeletons were sampled for Li/Mg and Ba/Ca ratios~~ (Fig. S1). Element concentrations were determined at the Institute for Geosciences, Johannes Gutenberg University Mainz (Germany), using an Agilent 7500ce inductively coupled plasma-mass spectrometer (ICP-MS) coupled to an ESI NWR193 ArF excimer laser ablation (LA) system equipped with a TwoVol2 ablation cell. The ArF LA system was operated at a pulse repetition rate of 10 Hz and an energy density of ca. 3 J cm^{-2}. Ablation was carried out under a He atmosphere and the sample gas was mixed with Ar before entering

150 the plasma. Measurement spots with a beam diameter of 120 µm were aligned along transects in spot mode with a midpoint distance of 250 µm following discrete skeletal elements. Backgrounds were measured for 15 s prior to each ablation. Ablation time was 30 s, followed by 20 s of wash out. The isotopes monitored were ^{7}Li, ^{25}Mg, ^{43}Ca and ^{138}Ba. Signals were monitored in time-resolved mode and processed using an in-house Excel spreadsheet (Jochum et al., 2007). Details of the calculations are given in Mischel et al. (2017). NIST SRM 610 and 612 were used as calibration material, applying the reference values

155 reported in the GeoReM database (http://georem.mpch-mainz.gwdg.de/, Application Version 27; Jochum et al., 2005; Jochum et al., 2011) to calculate the element concentrations of the sample measurements. During each run, basaltic USGS BCR-2G, synthetic carbonate USGS MACS-3 and a nano-powder pellet of biogenic carbonate JCp-1 (Garbe-Schönberg and Müller, 2014) were analysed repeatedly as quality control materials (QCM) to monitor precision and accuracy of the measurements as well as calibration strategy. All reference materials were analysed at the beginning and at the end of a sequence and after ca.

160 40 spots on the samples. For all materials ^{43}Ca was used as internal standard applying for the USGS BCR-2G and MACS-3 the preferred values reported in the GeoReM database, for JCp-1 38.18 wt.% (Okai et al., 2002) and for the samples a Ca content of 39 wt.% (Mertz-Kraus et al., 2009). Resulting element concentrations for the QCMs together with reference values are provided in the supplementary material (Table S1). Element concentrations for the samples are converted into molar ratios of Ca, i.e., Li/Ca, Mg/Ca, Ba/Ca as well as Li/Mg.

165 Li/Mg thermometry was used for estimating absolute growth temperatures (Montagna et al., 2014; Cuny-Guirriec et al., 2019, Ross et al., 2019b, Harthone et al., 2013; Fowell et al., 2016; D'Olivo et al., 2018; Zinke et al., 2019). Li/Mg - SST relationships were shown to be site dependent, however, and similar Li/Mg-ratios produce differences in SST estimations of ~2 °C between inter-reef (Hathorne et al., 2013) and intra-reef settings (Fowell et al., 2016). Such spatial variability in Li/Mg - SST relationships is likely due to poorly constrained effects of extension rate and seawater pH on skeletal Li/Mg ratios (Fowell et

170 al., 2016; Fowell, 2017; Inoue et al., 2007; Tanaka et al., 2015). For this reason, we use a separate calibration of the Li/Mg

thermometer for Masirah Island corals in order to overcome misleading SST estimates resulting from local seawater pH and extension rate effects associated with upwelling.

Ba/Ca ratios were used to identify skeletal portions calcified under upwelling conditions (Lea et al., 1989; Tudhope et al., 1996). Elevated Ba/Ca ratios in coral skeletons reflect high seawater Ba concentrations associated with upwelling deep waters,
175 which are also nutrient-rich and acidic (Fallon et al., 1999; Montaggioni et al., 2006).

Daily Sea surface temperatures (SST_{rem}) were extracted from JPL MUR (v4.1) available from https://podaac.jpl.nasa.gov. The JPL MUR data range used for this study covers the period 2003-2018 and has a spatial resolution of 0.01° degrees (Grid cell: N19.90, E58.60). SSTs of equal calendar dates of consecutive years were averaged receiving one generalized annual record of mean daily SSTs for the period 2003-2018 (Fig. 2). Reliability of the remote sensed data was confirmed by daily in-situ
180 observed SSTs ($SST_{in\text{-}situ}$) recorded at the southern tip of Masirah Island (water depth: 5 m) between October 2001 and September 2002 (Wilson, 2007). Annual mean SSTs were in excellent ~~accordance~~ agreement to each other (SST_{rem} = 25.79 °C ; $SST_{in\text{-}situ}$ = 25.54 °C) and daily SSTs were strongly correlated (r^2 = 0.79 , p < 0.0001).

Monthly seawater phosphate and nitrate concentrations come from the World Ocean Atlas 2018 (WOA18) available on https://www.nodc.noaa.gov/OC5/woa18/woa18data.html (Grid cell: N19.5, E58.5, water depth: 5 m; Fig. 2). The WOA18
185 nutrient data is a generalized interpolation of all available in-situ observations performed within individual months at certain depth levels within each 1° square (Garcia et al., 201~~8~~9).

Monthly interpolated seawater aragonite saturation states for the northern Arabian Sea (Grid cell: N16.0, E57.5; Fig.2) were extracted from https://www.ldeo.columbia.edu/res/pi/CO2/carbondioxide/pages/global_ph.html (Takahashi et al., 2014).

2.4 Data matching and age model development

190 Records of skeletal density and element concentrations of corals 5.10, 5.13 and 5.21 were matched with optical microscope images allowing for the correlation of ablated spots from LA-ICP-MS with distinctive features on X-radiographs. Slight offsets between the x-axis of the LA-ICP-MS record and the density records can occur, because to some extent the LA-ICP-MS sampling paths were not ultimately straight due to following discrete corallites and avoiding bioerosion traces and incrustations. To overcome this, the chronologies of the density records inferred from straight transects orientated parallel to
195 the direction of growth were applied to the LA-ICP-MS records using AnalySeries software (Paillard et al., 1996).

Age models are based on Li/Mg-ratios in combination with Ba/Ca-ratios. Li/Mg is inversely related to temperature, which allows to identify the two warm (intermonsoon) and two cool (monsoon) seasons (Harthone et al., 2013). In order to identify the upwelling season ~~(SWM)~~ among the two cool monsoons seasons (southwest monsoon, northeast monsoon)~~SWM and NEM~~, we use Ba/Ca ratios as proxy (Tudhope et al., 1996) (Fig. 3). A detailed chronological frame for the Li/Mg records was
200 established with the aid of the generalized annual record of remote sensing SST data (JPL MUR, daily averaged 2003 – 2018) (Fig. 2). Dates of seasonal SST extremes as well as dates of inflection points between consecutive seasons were assigned to corresponding data points of the Li/Mg records (see supplementary material, Fig. S2). This methodology allows tuning the age models to a total of eight tie-points per year (two per season). Dates between tie-points were interpolated linearly and the entire

time axis was resampled to monthly intervals using AnalySeries software (Paillard et al., 1996). Accuracy of the age model
was checked by comparing the timing of seasonal remote sensing SST maxima and minima of individual years with dates of
the generalized annual record (daily averages 2003-2018) and was found to be ± 4 weeks during ~~northeast monsoon~~NEM, ± 3
weeks during ~~spring intermonsoon~~SIM and ~~southwest monsoon~~SWM, and ± 1.5 weeks during ~~autumn intermonsoon~~AIM.

3 Results

3.1 Coral Ba/Ca and Li/Mg records

Multi-year monthly means of the Ba/Ca records show pronounced maxima within one annual cycle, which have been used in
establishing the age model to determine the southwest monsoonal upwelling season (Fig.3) (Tudhope et al., 1996; Lea at al.,
1989). Peak intensities vary considerably between samples, with coral 5.13 showing the lowest and coral 5.21 the highest
Ba/Ca ratios during upwelling. All individual Ba/Ca records are positively related with WOA18 seawater phosphate and nitrate
data (5.10: r^2 $_{(PO_4^{3-})}$ = 0.68, p = 0.0009; r^2 $_{(NO_3^-)}$ = 0.74, p = 0.0003; 5.13: r^2 $_{(PO_4^{3-})}$ = 0.84, p < 0.0001; r^2 $_{(NO_3^-)}$ = 0.94, p <
0.0001; 5.21: r^2 $_{(PO_4^{3-})}$ = 0.77, p = 0.0002; r^2 $_{(NO_3^-)}$ = 0.84, p < 0.0001) (Garcia et al., 201~~8~~9).
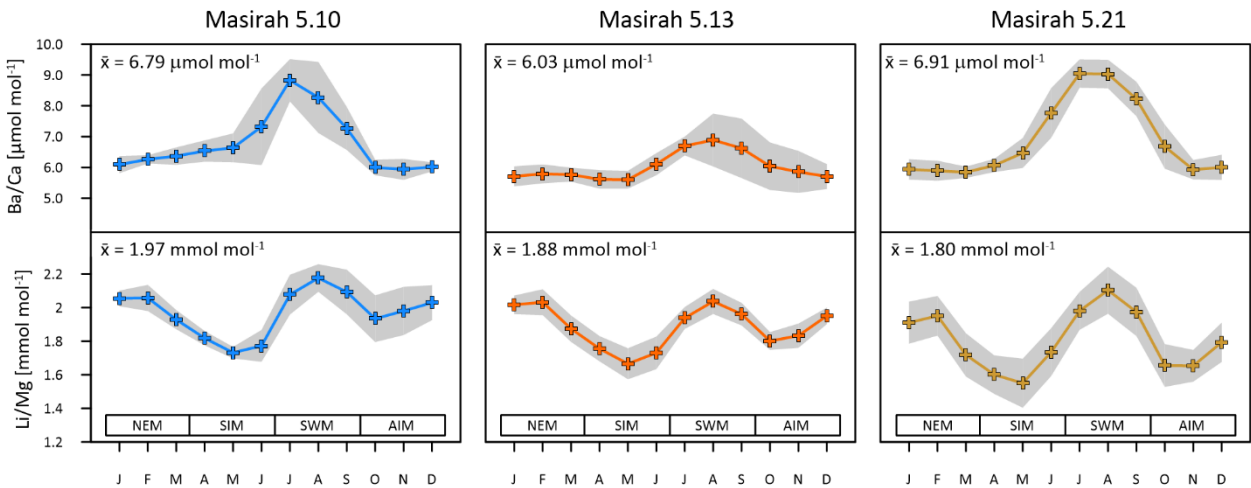
**Figure 3: Multi-year monthly means in Ba/Ca and Li/Mg of three Masirah corals (blue, orange, yellow). The grey shaded area
represents uncertainty (1σ) between equal months of consecutive years. Seasonal abbreviations: NEM (northeast monsoon), SIM
(spring intermonsoon), SWM (southwest monsoon), AIM (autumn intermonsoon).**

All multi-year monthly means of the Li/Mg records show pronounced patterns of two maxima and two minima within one
annual cycle (Fig. 3). Li/Mg maxima coincide with peaks in Ba/Ca during southwest monsoonal upwelling ~~(SWM)~~, while a
second, maximum of Li/Mg is reached during winter ~~(NEM)~~. Minima occur during the intermonsoon seasons ~~(SIM, AIM)~~.
All individual Li/Mg records exhibit the typical inverse relationship with monthly remote sensing SST data (JPL MUR) (5.10:
r^2 = 0.65, p = 0.0016; 5.13: r^2 = 0.75, p = 0.0003; 5.21: r^2 = 0.91, p < 0.0001).

Multi coral monthly means in Li/Mg are used for the calibration of the Li/Mg thermometer with mean monthly SSTs$_{rem}$ (averages of 2003-2018, JPL MUR) (Fig. 4). 83 % of the intra-annual multi coral monthly Li/Mg variation is explained by temperature and the resultant SST-calibration is estimated as:

230

$$\text{Li/Mg [mmol mol}^{-1}\text{]} \quad = -0.083\ (\pm 0.012) \times SST + 4.029\ (\pm 0.305) \quad (r^2 = 0.83; p < 0.0001) \quad \text{Eq. 1}$$
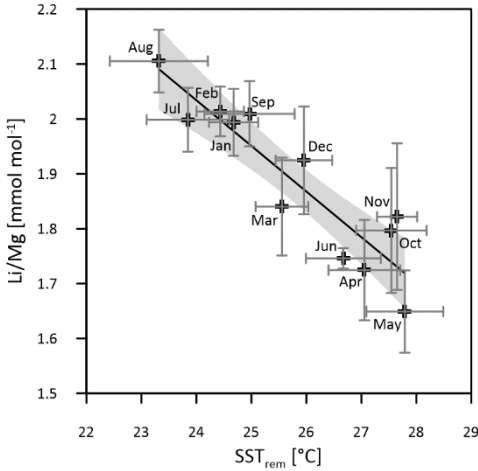
Figure 4: Multi coral calibration of the Li/Mg thermometer with SSTs$_{rem}$ (monthly means 2003-2018, JPL MUR). Horizontal error bars (1σ) represent SST uncertainty between equal months of consecutive years (2003-2018) and vertical error bars (1σ) represent
235 **uncertainty of multi-year monthly mean Li/Mg ratios between the three Masirah corals. The grey shaded area indicates the 95 % confidence interval of the linear regression.**

Table 1: Mean seasonal SSTs (± 1σ) inferred from multi-year monthly mean Li/Mg ratios of individual corals from Masirah Island. Uncertainty (1σ) represents variability between equal seasons of consecutive years. Seasonal abbreviations: NEM (northeast
240 **monsoon), SIM (spring intermonsoon), SWM (southwest monsoon), AIM (autumn intermonsoon).**

	5.10	5.13	5.21
	Li/Mg-SST [°C]	Li/Mg-SST [°C]	Li/Mg-SST [°C]
SIM	27.03 ± 0.45	27.85 ± 0.88	29.00 ± 1.25
SWM	23.03 ± 0.95	24.79 ± 0.74	24.36 ± 1.25
AIM	25.00 ± 1.28	26.08 ± 0.48	28.49 ± 0.80
NEM	24.13 ± 0.42	24.88 ± 0.57	25.72 ± 1.19

3.2 Pattern of calcification

Mean annual skeletal density, extension rate and calcification rate as well as the number of record years investigated within each of the six individual coral specimens is shown in Table 2. Sub-annually resolved patterns of calcification of coral 5.10,
245 5.13 and 5.21 are expressed as multi-year monthly means (Fig.5). The variability in monthly calcification rate within all three

specimens is strongly determined by extension rate (5.10: $r^2 = 0.94$, $p < 0.0001$; 5.13: $r^2 = 0.77$, $p < 0.0002$; 5.21: $r^2 = 0.81$, $p < 0.0001$). Coral 5.13 and 5.21 show three distinct peaks of highest extension rate in March, June and October. Reduced linear growth occurs during southwest monsoonSWM, northeast monsoonNEM as well as between April and May. Coral 5.10 slightly deviates from the pattern of the two other specimens by a lower growth rate during June, leading to two peaks of maximum extension in February/March and October. In this specimen, a decrease in linear growth starts in spring intermonsoonSIM and reaches its minimum during southwest monsoonSWM.

Sub-annual variability in skeletal bulk density of coral specimens 5.10 and 5.13 show a pattern of two distinct high density bands (HDBs) between two bands of low density (LDB) within one annual growth increment (Fig.5). Skeletal portions of low density were deposited during spring intermonsoonSIM and autumn intermonsoonAIM, high density portions formed during southwest monsoon SWM and northwest monsoonNEM. This alternating pattern of HDBs and LDBs causes skeletal density variation in coral 5.10 and 5.13 to be significantly inversely related to monthly reconstructed Li/Mg-SSTs (5.10: $r^2 = 0.87$, $p < 0.0001$; 5.13: $r^2 = 0.34$, $p < 0.05$) (Fig.6c). This is not the case for coral 5.21, as a well expressed LDB equivalent with autumn intermonsoonAIM is lacking. Rather, it shows one wide LDB with density increasing from southwest monsoonSWM to northeast monsoonNEM.

Table 2: Mean annual skeletal bulk density, linear extension rate and calcification rate ($\pm 1\sigma$) of all six coral specimens from Masirah Island. Uncertainty (1σ) represents variability between consecutive record years.

	Record years [n]	Bulk density [g cm^{-3}]	Extension rate [cm yr^{-1}]	Cacification rate [g cm^{-2} yr^{-1}]
5.9	6	1.03 ± 0.04	1.19 ± 0.16	1.22 ± 0.15
5.10	3	1.02 ± 0.02	1.43 ± 0.05	1.45 ± 0.08
5.13	5	0.91 ± 0.06	1.17 ± 0.12	1.03 ± 0.07
5.15	3	1.07 ± 0.04	1.07 ± 0.16	1.14 ± 0.14
5.21	5	0.99 ± 0.07	1.53 ± 0.11	1.49 ± 0.10
5.22	4	0.95 ± 0.05	1.47 ± 0.13	1.38 ± 0.08
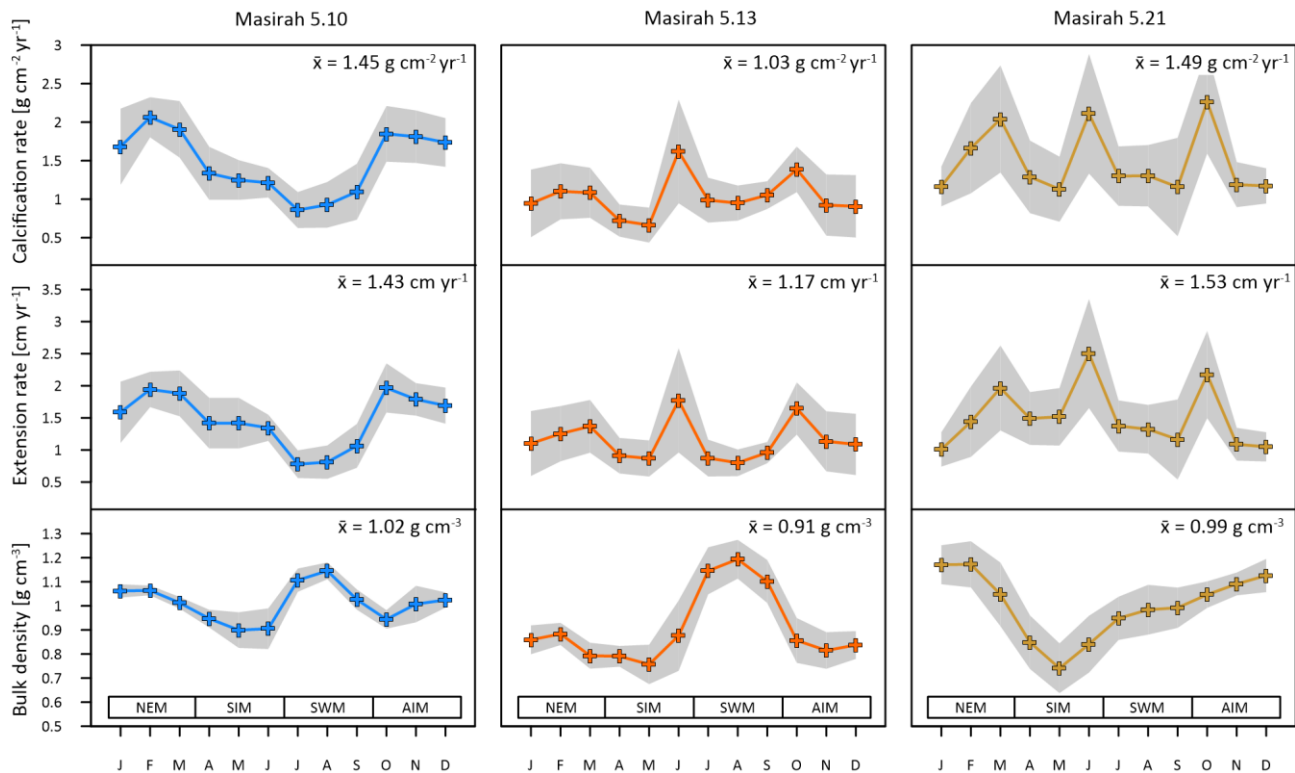
Figure 5: Results of multi-year monthly means of calcification rate, extension rate and skeletal density of three corals from Masirah Island (blue, orange, yellow). The grey shaded area represents uncertainty (1σ) between equal months of consecutive years. Seasonal abbreviations: NEM (northeast monsoon), SIM (spring intermonsoon), SWM (southwest monsoon), AIM (autumn intermonsoon).
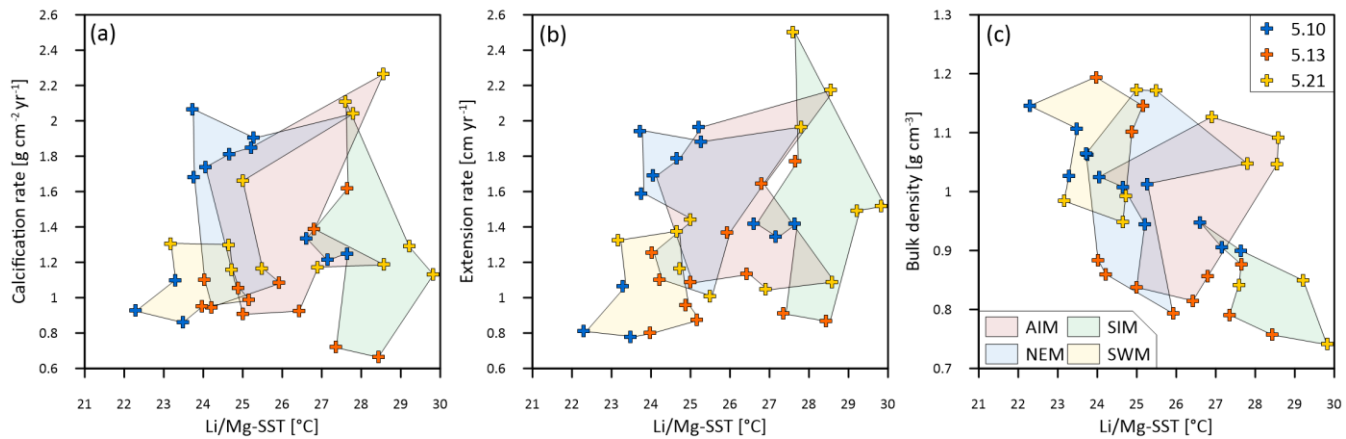
Figure 6: Multi-year monthly means of (a) calcification rate, (b) extension rate and (c) skeletal bulk density and associated Li/Mg-SSTs of three corals from Masirah Island (blue, orange, yellow). The coloured shaded polygons combine monthly data that belong to the same season. Seasonal abbreviations: NEM (northeast monsoon), SIM (spring intermonsoon), SWM (southwest monsoon), AIM (autumn intermonsoon).

275 Calcification rate during southwest monsoonSWM is only 51 %, 96 % and 78 % of that observed during NEM northwest monsoon (for coral 5.10, 5.13 and 5.21, respectively) (Table 3; Fig.6a). This difference in seasonal calcification rate is related to low extension rate during southwest monsoonal upwelling, which is 49 %, 71 % and 91 % relative to that observed during NEM northeast monsoon (for coral 5.10, 5.13 and 5.21, respectively). Interestingly, monthly extension rate during SWM southwest monsoon exhibit a strong negative correlation with skeletal density across all three specimen ($r^2 = 0.88$, p = 0.0002), 280 which is not the case during NEMnortheast monsoon ($r^2 = 0.04$, p = 0.60) (Fig.7). According to individual SWM extension rates during southwest monsoon, this produces varying density patterns across the three specimens, with corals 5.13 and 5.10 having the lowest SWM extension rate during southwest monsoon showing the highest intra-annual skeletal density during this season (Table 3; Fig.5). Coral 5.21 that shows relatively fast SWM extension growth during southwest monsoon compared to all other specimens only reveals a moderate increase in skeletal density, which remains below those observed during the 285 NEMnortheast monsoon.

Table 3: Mean seasonal skeletal bulk density, linear extension rate and calcification rate (± 1σ) of three corals from Masirah Island. Uncertainty (1σ) represents variability between equal seasons of consecutive years. Seasonal abbreviations: NEM (northeast monsoon), SIM (spring intermonsoon), SWM (southwest monsoon), AIM (autumn intermonsoon).

	5.10			5.13			5.21		
	Bulk density [g cm^{-3}]	Extension rate [cm yr^{-1}]	Cacification rate [g cm^{-2} yr^{-1}]	Bulk density [g cm^{-3}]	Extension rate [cm yr^{-1}]	Cacification rate [g cm^{-2} yr^{-1}]	Bulk density [g cm^{-3}]	Extension rate [cm yr^{-1}]	Cacification rate [g cm^{-2} yr^{-1}]
SIM	0.94 ± 0.04	1.26 ± 0.23	1.18 ± 0.20	0.81 ± 0.07	1.25 ± 0.34	1.02 ± 0.25	0.80 ± 0.1	1.83 ± 0.30	1.47 ± 0.33
SWM	1.10 ± 0.01	0.87 ± 0.06	0.95 ± 0.06	1.15 ± 0.08	0.90 ± 0.18	1.02 ± 0.18	0.94 ± 0.05	1.31 ± 0.23	1.24 ± 0.28
AIM	0.99 ± 0.03	1.83 ± 0.28	1.81 ± 0.33	0.83 ± 0.07	1.25 ± 0.27	1.03 ± 0.21	1.09 ± 0.06	1.55 ± 0.20	1.65 ± 0.19
NEM	1.05 ± 0.01	1.79 ± 0.17	1.88 ± 0.17	0.85 ± 0.05	1.26 ± 0.31	1.06 ± 0.26	1.12 ± 0.1	1.44 ± 0.20	1.58 ± 0.11

290
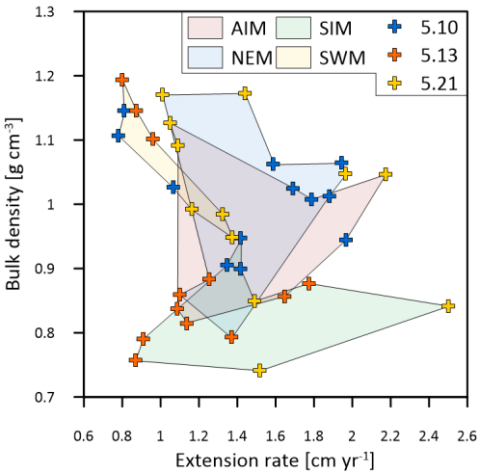
Figure 7: Multi-year monthly means in extension rate versus skeletal bulk density of the three corals from Masirah Island (blue, orange, yellow). The coloured shaded polygons combine monthly data that belong to the same season. Seasonal abbreviations: NEM (northeast monsoon), SIM (spring intermonsoon), SWM (southwest monsoon), AIM (autumn intermonsoon).

4 Discussion

4.1 Ba/Ca records

Multi-year monthly means in skeletal Ba/Ca are in excellent agreement with WOA18 nutrient data. This confirms Ba/Ca to be an appropriate proxy for intra-annual variability in seawater nutrient concentrations (Fallon et al., 1999; Montaggioni et al., 2006). Effects of riverine input on the skeletal Ba/Ca record can be excluded due to the absence of rivers in the arid region of north-eastern Oman (Alibert et al., 2003; Jiang et al., 2017). This allows intra-annual variability in Ba/Ca to be fully attributed to upwelling (Tudhope et al., 1996; Lea et al., 1989). Variable Ba/Ca ratios across specimens during southwest monsoonal upwelling season ~~(SWM)~~ are likely to result from spatial heterogeneous seawater barium distribution within the reef.

4.2 Li/Mg records

SST reconstructions based upon the calibration of the Li/Mg thermometer described above (Eq. 1) reproduce the monthly cur~~ve~~se of the SST_{rem} data ($r^2 = 0.83$, $p < 0.0001$) as well as observed $SST_{in\text{-}situ}$ variations at Masirah Island ($r^2 = 0.93$, $p < 0.0001$) (Wilson, 2007). Temperature sensitivity of the Li/Mg-thermometer deduced from reconstructed seasonality is in good agreement with the majority of proxy calibration studies from the literature (Hathorne et al., 2013; Ross et al., 2019b; Cuny-Guirriec et al., 2019; Montagna et al., 2014; Fowell et al., 2016 ~~(Forereef)~~). The intercept of the linear Li/Mg-SST calibration of the Masirah corals, however, is 4-5 °C higher than reported in the literature (Fig. 8). Analytical uncertainties that noticeably bias the Li/Mg ratio are unlikely as a source for high Li/Mg ratios, because systematic measurement discrepancies deduced from the JCp-1 QCM for Li/Ca and Mg/Ca would rather tend to underestimate the Li/Mg ratios (Li/Ca: +4.44 % ; Mg/Ca: +7.37 %; Table S1). In addition to temperature, seawater pH also has shown to bias the skeletal Li/Mg ratio of corals (Fowell et al., 2016; Fowell, 2017; Tanaka et al., 2015). For identical SSTs, culture experiments on *Sideastrea siderea* show an increase of 0.325 mmol/mol in Li/Mg per decreasing pH_{sw} unit (Fowell, 2017). However, comparatively high Li/Mg values found in the Masirah corals are present year-round, while exceptionally low pH_{sw} is limited to the three monthly southwest monsoon upwelling season (Omer, 2010; Takahashi et al., 2014). This suggests that skeletal Li/Mg is not directly sensitive to the external pH_{sw}, but rather to the carbonate chemistry of the calcification fluid, which through modification is independent of external variations in pH_{sw} (McCulloch et al., 2017). Conditions within the calcifying fluid must permanently alter skeletal Li/Mg of *Porites* at Masirah Island towards higher values compared to published SST-Li/Mg calibrations reported in the literature, which might imply year-round stable but low pH_{cf}.
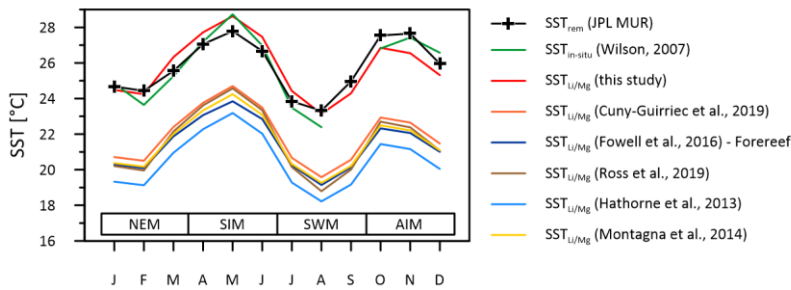
Figure 8: Instrumental SSTs (green line) compared to multi coral monthly mean SSTs inferred from Li/Mg ratios of the Masirah corals using the calibration of this study (red line) and calibrations reported from the literature. Published Li/Mg-SST calibrations cause variable degrees of underestimation of ~~coral growth temperatures~~reconstructed SST at Masirah Island. Seasonal abbreviations: NEM (northeast monsoon), SIM (spring intermonsoon), SWM (southwest monsoon), AIM (autumn intermonsoon).

4.3 Skeletal calcification

4.3.1 Monthly records of coral calcification

Monthly variability in calcification rate is largely driven by extension rate across all samples (Fig.5), similar to that reported for *Porites* from the Indo-Pacific region (Lough and Barnes, 2000). However, the typical positive correlation between monthly extension rate and SST does not exist in our data (Fig.6b). All three specimens reveal noticeably small extension growth during April and May despite ~~of~~ high ~~SIM~~ temperatures during spring intermonsoon. Interestingly, coral spawning at Omani reef sites is reported to take place between March and May (Howells et al., 2014). Correspondingly, a reduction of extension rate during spring intermonsoon~~SIM~~ could be linked to high-energy expenditures required for reproduction (Cabral-Tena et al., 2013).

All specimens show lower ~~SWM~~ calcification rate during southwest monsoon compared to that observed for ~~NEM~~the northeast monsoon, which is attributed to smaller extension rate during the upwelling (Table 3). Declining extension rate during upwelling season is in agreement with growth studies on *Pocillopora damicornis* from the Gulf of Panama (Glynn, 1977). For corals from Masirah Island, at least part of the seasonal difference in extension rate between southwest monsoon~~SWM~~ and northeast monsoon~~NEM~~ might be related to slightly lower SSTs during the southwest monsoonal upwelling (Table 1). Given an increase in extension rate of 0.33 cm yr^{-1} per 1°C as suggested for Indo-Pacific *Porites*, differences in extension rate between southwest monsoon~~SWM~~ and northeast monsoon~~NEM~~ could be fully explained by temperature for coral 5.21, but only to some extent for coral 5.10 and 5.13 (Lough and Barnes, 2000). Intens~~eive~~ eutrophication might have additional impact on growth of Masirah corals, with detrimental effects on extension rate during the upwelling season (Tomascik, 1990). Assuming direct detrimental effects of the essential nutrients on coral growth, the inhibiting effect of NO_3^- would have to outweigh the promoting effect of PO_4^{3-} on southwest monsoon~~SWM~~ extension rate of the Masirah corals (Koop et al., 2001; Dunn et al., 2012; Bucher and Harrison, 2001). However, the northern Arabian Sea is characterized by a high PO_4^{3-} to NO_3^- ratio, making this direct effect of nutrients on the extension rate unlikely (Kleypas, 1999). As a general consequence of the excessively high nutrient concentrations, primary productivity in the Arabian Sea increases rapidly during the upwelling season, leading to high levels of turbidity associated with low light transparency of the water column (Anderson et al., 1992; Bauer et al., 1991; Quinn

and Johnson, 1996). Reduced photosynthetic efficiency of the micro-algae symbionts seems to be a potential factor for diminished extension rate in response to reduced energy reserves during upwelling (Al Shehhi et al., 2014; Logan and Tomascik, 1991; Muscatin et al., 1981; Sun et al., 2008; Tomascik, 1990). Energy through heterotrophic feeding does not seem to be sufficient for Masirah corals to fully compensate for reduced levels of photosynthates (Tomascik and Sander, 1985). Interestingly, highest monthly extension rate occur immediately before and after the upwelling season during June and October, respectively (Fig.5). A decrease in the extension rate during the southwest monsoonSWM sets on immediately at the beginning of the upwelling, only to recover rapidly again afterwards. We therefore conclude that the coral's energy reserves available for skeletal upward growth response instantaneous to monthly environmental changes (i.e., turbidity), without delays or extended times for recovery.

In contrast to *Porites* from the Indo-Pacific region, which showing only a moderate dependence of skeletal density on SST, Li/Mg-SSTs at Masirah Island are strongly correlated with the monthly variation in skeletal density in coral 5.10 and 5.13 (Lough and Barnes, 2000). This is however not observed for coral 5.21, as a weakly developed HDB during southwest monsoonSWM worsens a causal relationship with SST (Fig.6c). This comparatively low density during southwest monsoonal upwelling coincides with relatively high SWM extension rate in coral 5.21 compared to all other samples (Table 3; Fig.6b). Excellent negative correlation between southwest monsoonal data of monthly density and extension rate across the three corals (n = 9, r^2 = 0.88, p = 0.0002) indicates density during upwelling to be substantially controlled by extension rate (Fig.7). A simple model in which the active calcification surface to which $CaCO_3$ is accreted is relatively large at high extension rate, resulting in thin skeletal elements and low bulk density (and vice versa for HDBs) might explain inter-specimen variability in skeletal density patterns of the Masirah corals during southwest monsoonSWM (DeCarlo and Cohen, 2017). No evidence supports an immediate detrimental impact of upwelling, i.e., a temporally low Ω_{sw}, on sub-annual patterns in skeletal density. Given that density is likely being controlled by the carbonate chemistry of the calcification fluid, we propose Ω_{cf} is kept relatively constant by modification independent of external variations in Ω_{sw} during upwelling and non-upwelling seasons (DeCarlo et al., 2018; McCulloch et al., 2017; Mollica et al., 2018).

4.3.2 Annual records of coral calcification

The mMean annual calcification rate at Masirah Island is indistinguishable from those of *Porites* from Indo-Pacific and Atlantic reef sites, which are unaffected by upwelling (Fig.9a). A similar finding is reported from two sites located within the Galapagos upwelling zone (n = 7-8 cores per site) (Manzello et al., 2014). Although a pPoor replication of *Porites* calcification data from the upwelling areas of Panama and the South China Sea (n = 1, respectively) does not enable a proper comparison (Mollica et al., 2018). , statistically robust data reported from two sites located within the Galapagos upwelling zone (n = 7-8 cores per site) reveal an identical result (Manzello et al., 2014; Mollica et al., 2018). PHowever, patterns of calcification in *Porites* from Masirah Island and Galapagos differ from those found in regions without upwelling by showing enhanced extension rate andt

~~concurrently~~ lower skeletal density, similar to the pattern termed "stretching modulation of skeletal growth" by Carricart-Ganivet (2004) (Fig.9b, 9c). High mean annual *Porites* extension rate at Galapagos was discussed as potential impact of the stimulating effects of ~~is discussed by the authors in terms of the stimulating effect of~~ nutrients on upward growth (Manzello et al., 2014). Nutrient-stimulated growth is also suggested for enhanced annual extension growth of *Pocillopora damicornis* and *Pavona clavus* from the Panama upwelling zone compared to data from regions unaffected by upwelling (Glynn, 1977; Wellington and Glynn, 1983). In fact, enhanced annual extension rate of *Pavona clavus* from Panama is the result of high extension growth during the non-upwelling season, similar to the pattern seen in ~~a pattern also applicable to the herein presented~~ *Porites* from Masirah Island (Wellington and Glynn, 1983) (Table 3). Hence, a stimulating effect of nutrients on extension rate during the non-upwelling seasons is possible, ~~in particular because in the northern Arabian Sea~~since moderate nutrient concentrations with high PO_4^{3-} to NO_3^- ratio exist year-round in the Arabian Sea (Dunn et al., 2012; Kleypas et al., 1999; Koop et al., 2001).

Low skeletal density of coral specimens from Masirah Island is consistent with low skeletal density reported in the literature for *Porites* from the upwelling regions of the eastern Pacific and the China Sea (Mollica et al., 2018; Manzello et al., 2014) (Fig.9c). Boron isotope analyses on some of these samples have revealed the low skeletal density to be driven by a relatively low Ω_{cf} compared to corals from regions unaffected by upwelling (Mollica et al., 2018). Low Ω_{cf} in these specimens is maintained year-round, independent of external variations in Ω_{sw} (i.e., seasonal upwelling) (~~N. Mollica, personal communication, 2021~~Fig. S3). Accordingly, we hypothesise the year-round relatively low skeletal density of the Masirah corals to be also related to a constantly low Ω_{cf}.~~With regard to relatively low skeletal density of the Masirah corals, which persists year round and does not show an immediate response to SWM upwelling, we consider transferring the same mechanism of a constant low Ω_{cf}.~~ This ~~argument is also~~hypothesis is further supported by the Li/Mg ratios of the Masirah corals, which are offset to higher values than those expected from the literature (Fig.8). As this offset is present throughout the year, it cannot be attributed to temporarily low pH_{sw} associated to seasonal upwelling, but rather reflects year-round constant conditions within the calcifying fluid (Fowell, 2017; McCulloch et al., 2017). This finding implies that there is no intensified upregulation of internal Ω_{cf} relative to Ω_{sw} during the non-upwelling seasons (McCulloch et al., 2017; DeCarlo et al., 2018; D'Olivo and McCulloch, 2017). As an explanation, we propose that internal upregulation processes of corals affected by seasonal upwelling are not capable to adapt completely to ocean chemistry change on a quarterly scale. As a consequence, a relatively low Ω_{cf} could be~~is~~ maintained year-round so as to avoid high gradients to the external Ω_{sw} during southwest monsoonal upwelling.
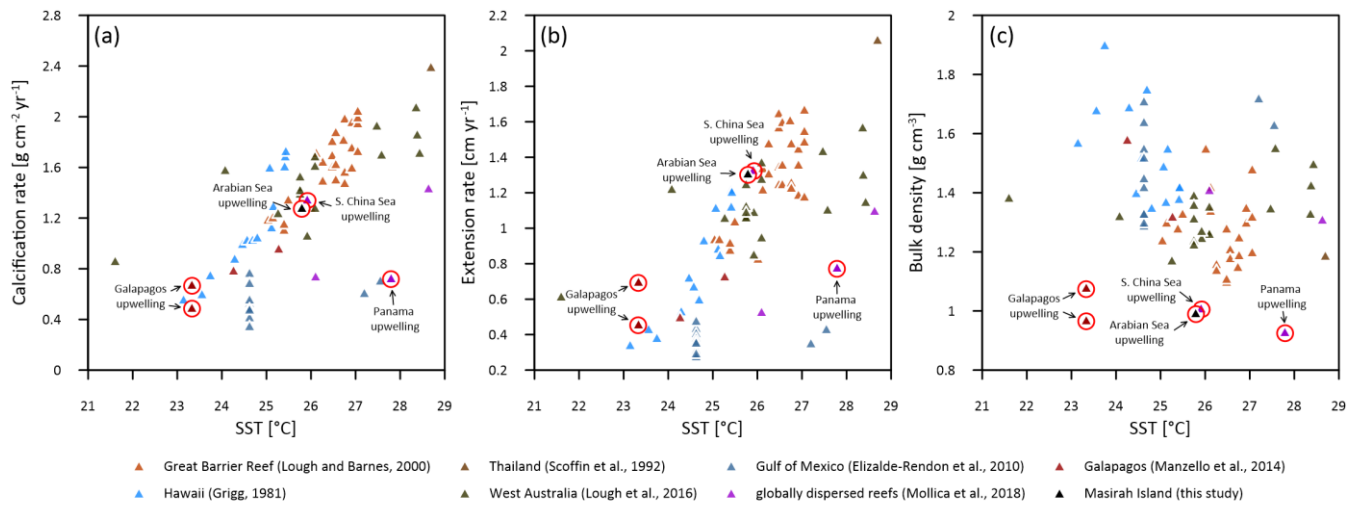
Figure 9: Annual means of *Porites* calcification rate (a), extension rate (b) and skeletal bulk density (c) versus sea surface temperature (SST) from various Indo-Pacific and Western Atlantic reef sites. Red circles indicate sites affected by seasonal upwelling.

5 Conclusion

This study investigates the effect of seasonal upwelling on sub-annual and annual patterns of calcification in reef corals (*Porites*) from the northern Arabian Sea (Masirah Island, Oman). On a sub-annual basis, calcification rate is lower during the upwelling season compared to periods of near identical SST in the non-upwelling season. This is attributed to a rapid decline in extension rate with the onset of the upwelling season. We attribute this decline to a reduction of photosynthetic performance of the micro-algae symbionts potentially caused by enhanced turbidity of ambient seawater through elevated primary production. Patterns of skeletal density do not exhibit an no instantaneous response to the external decline in Ω_{sw} during upwelling, which indicates stable levels of Ω_{cf} to be maintained throughout the year. Nonetheless, mean annual skeletal density is significantly lower than in *Porites* from typical reef environments of the Indo-Pacific and Atlantic Ocean. In contrast, mean annual extension rate is high, likely due to the simulating effect of moderate seawater nutrient concentrations during the non-upwelling seasons. As high extension rate compensates for the deficit in skeletal density at Masirah Island, annual calcification rate is indistinguishable from *Porites* growing in regions unaffected by upwelling.

These results suggest that temporarily reduced Ω_{sw} (seasonal upwelling) has no instantaneous impact on sub-annual variability in skeletal density but could causes a permanent adaptation towards year-round unexpected low skeletal density. Unless the low skeletal density is compensated through high extension rate, this will yield detrimental effects on the net carbonate accumulation in coral reefs. Furthermore, this study highlights variable effects of nutrients on extension rate, with negative effects at excessively high nutrient levels (i.e., upwelling season) and stimulatory effects at moderate nutrient levels (i.e., non-upwelling season).

Further research should include combined analyses of $\delta^{11}B$ and B/Ca ratios in order to confirm the hypothesis of a year-round relatively low Ω_{cf} in reef corals from sites affected by seasonal upwelling.

Authors contribution

P. M. Spreter designed this research in close collaboration with T. C. Brachert and M. Reuter. Field work was carried out by P. M. Spreter, T. C. Brachert, M. Reuter and substantially supported by O. Taylor. Laboratory analyses were performed by P. M. Spreter and R. Mertz-Kraus. All authors had a contribution in writing and improving the manuscript.

Competing interests

The authors declare that they have no conflict of interest.

Acknowledgements

We are grateful to the Ministry of Environment and Climate Affairs (Muscat, Oman) for approving sampling and export permission (Permit numbers: 6210/10/44 and 177/2018). We kindly thank M.A. Claereboudt (Sultan Qaboos University, Muscat, Oman) for his support. Funding by the Deutsche Forschungsgemeinschaft (DFG, grant BR 1153/20-1, -2 and ME 3761/4-1) is gratefully acknowledged. The comments and ideas of three anonymous reviewers and Editor Tyler Cyronak greatly improved this manuscript.

References

Al-Rousan, S.:. Skeletal extension rate of the reef building coral *Porites* species from Aqaba and their environmental variables. Nat. Sci., 04, 731-739, https://doi.org/10.4236/ns.2012.49097, 2012.

Al Shehhi, M.R., Gherboudj, I., Ghedira, H.: An overview of historical harmful algae blooms outbreaks in the Arabian Seas. Mar. Pollut. Bull., 86, 314-324, https://doi.org/10.1016/j.marpolbul.2014.06.048, 2014.

Alibert, C., Kinsley, L., Fallon, S.J., McCulloch, M.T., Berkelmans, R., McAllister, F.: Source of trace element variability in Great Barrier Reef corals affected by the Burdekin flood plumes. Geochim. Cosmochim. Acta, 67, 231-246, https://doi.org/10.1016/S0016-7037(02)01055-4, 2003.

Anderson, D.M., Brock, J.C., Prell, W.L.: Physical upwelling process, upper ocean environment and the sediment record of the southwest monsoon. Upwelling systems: Evolution since the early Miocene. Geol. Soc. Spec. Publ., 64, 121-129, https://doi.org/10.1144/GSL.SP.1992.064.01.08, 1992.

Barrot, K.T., Rohwer, F.L.: Unseen players shape benthic competition on coral reefs. Trends Microbiol., 20, 621-628, http://doi.org/10.1016/j.tim.2012.08.004, 2012.

465   Bauer, S., Hitchcock, G.L., Olson, D.B.: Influence of monsoonally-forced Ekman dynamics upon surface layer depth and plankton biomass distribution in the Arabian Sea. Deep-Sea Res., 38, 531-553, https://doi.org/10.1016/0198-0149(91)90062-K, 1991.

Beal, L.M., Hormann, V., Lumpkin, R., Foltz, G.R.: The response of the surface circulation of the Arabian Sea to monsoonal
470   forcing. J. Phys. Oceanogr., 43, 2008-2022, https://doi.org/10.1175/JPO-D-13-033.1, 2013.

Bucher, D.J., Harrison, P.L.: Growth response of the reef coral *Acropora longicyathus* to elevated inorganic nutrients: do responses to nutrients vary among coral taxa? Proceedings 9th International Coral Reef symposium, Bali, Indonesia. 443-448, 2001.
475

Burt, J.A., Coles, S., van Lavieren, H., Taylor, O., Looker, E., Samimi-Namin, K.: Oman's coral reefs: A unique ecosystem challenged by natural and man-related stresses and in need of conservation. Mar. Pollut. Bull., 105, 498-506, 10.1016/j.marpolbul.2015.11.010, 2016.

480   Cabral-Tena, R.A., Reyes-Bonilla, H., Lluch-Cota, S., Paz-García, D.A., Calderón-Aguilera, L.E., Norzagaray-López, O., Balart, E.F.: Different calcification rates in males and females of the coral *Porites panamensis* in the Gulf of California. Mar. Ecol. Prog. Ser., 476, 1-8, https://doi.org/10.3354/meps10269, 2013.

Camp, E.F., Schoepf, V., Mumby, P.J., Hardtke, L.A., Rodolfo-Metalpa, R., Smith, D.J., Suggett, D.J.: The future of coral
485   reefs subject to rapid climate change: Lessons from natural extreme environments. Front. Mar. Sci., 5, 1-21, https://doi.org/10.3389/fmars.2018.00004, 2018.

Cantin, N.E., Cohen, A.L., Karnauskas, K.B., Tarrant, A.M., McCorkle, D.C.: Ocean warming slows coral growth in the central Red Sea. Science, 329, 322-325, http://doi.org/10.1126/science.1190182, 2010.
490

Carricart-Ganivet, J.P., Merino, M.: Growth responses of the reef-building coral *Montastraea annularis* along a gradient of continental influence in the southern Gulf of Mexico. Bull. Mar. Sci., 68, 133-146, 2001.

Carricart-Ganivet, J.P.: Sea surface temperature and the growth of the West Atlantic reef-building coral *Montastraea*
495   *annularis*. J. Exp. Mar. Bio. Ecol., 302, 249-260, http://doi.org/10.1016/J.JEMBE.2003.10.015, 2004.

Chen, M., Martin, P., Goodkin, N.F., Tanzil, J., Murty, S., Wiguna, A.A.: An assessment of P specification and P:Ca proxy calibration in coral cores from Singapore and Bali. Geochim. Cosmochim. Acta, 267, 113-123, http://doi.org/10.17632/2hbxk2njfx.1, 2019.
500

Chen, T., Yu, K.: P/Ca in coral skeleton as a geochemical proxy for seawater phosphorus variation in Daya Bay, northern South China Sea. Mar. Pollut. Bull., 62, 2114-2121, https://doi.org/10.1016/j.marpolbul.2011.07.014, 2011.

Coles, S.L., 1996. Corals of Oman. R.Keech, Thornes, Hawes, North Yorkshire, 106 pp.
505

Cornwall, C.E., Comeau, S., Kornder, N.A., Perry, C.T., van Hooidonk, R., DeCarlo, T.M., Pratchett, M.S., Anderson, K.D., Browne, N., Carpenter, R., Diaz-Pulido, G., D'Olivo, J.P., Doo, S.S., Figueiredo, J., Fortunato, S.A.V., Kennedy, E., Lantz, C.A., McCulloch, M.T., González-Rivero, M., Schoepf, V., Smithers, S.G., Lowe, R.J.: Global declines in coral reef calcium carbonate production under ocean acidification and warming. Proc. Natl. Acad. Sci. U. S. A., 118,
510   https://doi.org/10.1073/pnas.2015265118, 2021.

Cuny-Guirriec, K., Doouville, E., Reynaud, S., Allemand, D., Bordier, L., Canesi, M., Mazzoli, C., Taviani, M., Canese, S., McCulloch, M., Trotter, J., Rico-Esenaro, S.D., Sanchez-Cabeza, J.A., Ruiz-Fernández, A.C., Carricart-Garnivet, J.P.,

Scott, P.M., Sadekov, A., Montagna, P.: Coral Li/Mg thermometry: Caveats and constrains. Chem. Geol., 532, 162-178, https://doi.org/10.1016/j.chemgeo.2019.03.038, 2019.

Currie, R.I., Fisher A.E., Hargreaves P.M.: Arabian Sea Upwelling. In: Zeitzschel B., Gerlach S.A., The Biology of the Indian Ocean. Ecological Studies (Analysis and Synthesis) 3. Springer, Berlin, Heidelberg, http://doi.org/10.1007/978-3-642-65468-8, 1973.

Currie, R.I.: Circulation and upwelling off the coast of South-East Arabia. Oceanol. Acta, 15, 43-60, doi: , 1992.

D'Olivo, J.P., McCulloch, M.T., Judd, K.: Long-term records of coral calcification across the central Great Barrier Reef: assessing the impact of river runoff and climate change. Coral Reefs, 32, 999-1012, http://doi.org/10.1007/s00338-013-1071-8, 2013.

D'Olivo, J.P., McCulloch, M.: Response of coral calcification and calcifying fluid composition to thermally induced bleaching stress. Sci. Rep., 7, 1-15, http://doi.org/10.1038/s41598-017-02306-x, 2017.

D'Olivo, J.P., Sinclair, D.J., Rankenburg, K., McCulloch, M.T.: A universal multi-trace element calibration for reconstructing sea surface temperatures from long-lived Porites corals: Removing "vital effects". Geochim. Chosmochim. Acta, 239, 109-135, https://doi.org/10.1016/j.gca.2018.07.035, 2018.

D'Olivo, J.P., Ellwood, G., DeCarlo, T.M., McCulloch, M.T.: Deconvolving the long-term impacts of ocean acidification and warming on coral biomineralisation. Earth Planet. Sci. Lett., 526, 115785, https://doi.org/10.1016/j.epsl.2019.115785, 2019.

DeCarlo, T.M., Cohen, A.L.: Dissipiment, density bands and signatures of thermal stress in *Porites* skeletons. Coral reefs, 36, 749-761, http://doi.org/10.1007/s00338-017-1566-9, 2017.

DeCarlo, T.M., Comeau, S., Cornwall, C.E., McCulloch, M.T.: Coral resistance to ocean acidification linked to increased calcium at the site of calcification. Proc. Biol. Sci., 285, 1-7, https://doi.org/10.1098/rspb.2018.0564, 2018.

Dodge, R.E., Brass, G.W.: Skeletal extension, density and calcification of the reef coral, *Montastrea annularis*: St. Croix, U.S. Virgin Islands. Bull. Mar. Sci., 34, 288-307, doi: , 1984.

Dunn, J.G., Sammarco, P.W., LaFleur Jr, G.: Effects of phosphate on growth and skeletal density in the scleractinian coral *Acropora muricata*: A controlled experimental approach. J. Exp. Mar. Biol. Ecol., 411, 34-44, https://doi.org/10.1016/j.jembe.2011.10.013, 2012.

Elizalde-Rendón, E.M., Horta-Puga, G., González-Diaz, P., Carricart-Ganivet, J.P.: Growth characteristics of the reef-building coral *Porites astreoides* under different environmental conditions in the Western Atlantic. Coral Reefs, 29, 607-614, https://doi.org/10.1007/s00338-010-0604-7, 2010.

Fallon, S.J., McCulloch, M.T., Van Woesik, R., Sinclair, D.J.: Corals at their latitudinal limits: Laser ablation trace element systematics in *Porites* from Shirigai Bay, Japan. Earth Planet. Sci. Lett., 172, 221-238, https://doi.org/10.1016/S0012-821X(99)00200-9, 1999.

Findlater, J.: A major low-level air current near the Indian Ocean during the northern summer. Q. J. R. Meteorol. Soc., 95, 362-380, https://doi.org/10.1002/qj.49709540409, 1969.

Fowell, S.E., Sandford, K., Stewart, J.A., Castillo, K.D., Ries, J.B., Foster, G.L.: Intrareef variations in Li/Mg and Sr/Ca sea surface temperature proxies in the Caribbean reef-building coral *Siderastrea siderea*. Paleoceanography, 31, 1315-1329, https://doi.org/10.1002/2016PA002968, 2016.

565

Fowell, S.E.: Assessing the magnitude of anthropogenic ocean warming and ocean acidification using the novel Li/Mg-SST and δ^{11}B-pH proxies in the Caribbean coral *Siderastrea siderea*. Doctoral thesis. University of Southampton. 2017.

Fritz, H.M., Blount, C.D., Albusaidi, F.B., Al Harthy, A.H.M.: Cyclone Gonu storm surge in Oman. Estuar. Coast. Shelf Sci., 86, 102-106, http://doi.org/10.1007/978-90-481-3109-9_30, 2010.

570

Garbe-Schönberg, D., Müller, S.: Nano-particulate pressed powder tablets for LA-ICP-MS. J. Anal. At. Spectrom., 29, 990-1000, http://dx.doi.org/10.1039/C4JA00007B, 2014.

575 Garcia, H. E., Weathers, K., Paver, C. R., Smolyar, I., Boyer, T. P., Locarnini, R. A., Zweng, M. M., Mishonov, A. V., Baranova, O. K., Reagan, J. R.: World Ocean Atlas 2018, 4: Dissolved Inorganic Nutrients (phosphate, nitrate, silicate), 2019.

Glynn, P.W.: Monsoonal upwelling and episodic *Acanthaster* predation as probable controls of coral reef distribution and community structure in Oman, Indian Ocean. Atoll Res. Bull., 379, 1-66, https://doi.org/10.5479/si.00775630.379.1, 1993.

580

Guan, Y., Hohn, S., Wild, C., Merico, A.: Vulnerability of global coral reef habitat suitability to ocean warming, acidification and eutrophication. Glob. Chang. Biol., 26, 5646–5660, https://doi.org/10.1111/gcb.15293, 2020.

585

Grigg, W.G.: Coral reef development at high latitudes in Hawaii. Proceedings of the Fourth International Coral Reef Symposium, Manila, 1, 688-693, 1981.

Hall, E.R., Muller, E.M., Goulet, T., Bellworthy, J., Ritchie, K.B., Fine, M.: Eutrophication may compromise the resilience of the Red Sea coral Stylophora pistillata to global change. Mar. Pollut. Bull., 131, 701-711, https://doi.org/10.1016/j.marpolbul.2018.04.067, 2018.

590

Hallock, P.: The role of nutrient availability in bioerosion: Consequences to carbonate buildups. Palaeogeogr., Palaeoclimatol., Palaeoecol., 63, 275-291, https://doi.org/10.1016/0031-0182(88)90100-9, 1988.

595

Hastenrath, S., Greischar, L.: The monsoonal current regimes of the tropical Indian Ocean: Observed surface fields and their geostrophic and wind-driven components. J. Geophys. Res., 96, 12619-12633, http://doi.org/10.1029/91JC00997, 1991.

Hathorne, E.C., Felis, T., Suzuki, A., Kawahata, H., Cabioch, G.: Lithium in the aragonite skeleton of massive *Porites* corals: A new tool to reconstruct tropical sea surface temperatures. Paleoceangraphy, 28, 143-152, http://doi.org/10.1029/2012PA002311, 2013.

600

Helmle, K. P., Kohler, K. E., and Dodge, R. E., The coral X- radiograph densitometry system: CoralXDS, Nova Southeastern University, Fort-Lauderdale-Davie, 2002.

605

Helmle, K.P., Dodge, R.E., Swart, P.K., Gledhill, D.K., Eakin, C.M.: Growth rates of Florida corals from 1937 to 1996 and their response to climate change. Nat. Commun., 2, 215-216, http://doi.org/10.1038/ncomms1222, 2011.

Highsmith, R.C.: Coral growth rate and environmental control of density banding. J. Exp. Mar. Biol. Ecol., 37, 105-125, https://doi.org/10.1016/0022-0981(79)90089-3, 1979.

610

Howells, E.J., Abrego, D., Vaughan, G.O., Burt, J.A.: Coral spawning in the Gulf of Oman and relationship to latitudinal variation in spawning season in the northwest Indian Ocean. Sci. Rep., 4, 1-6, http://doi.org/10.1038/srep07484, 2014.

615 Hughes, T.P., Barnes, M.L., Bellwood, D.R., Cinner, J.E., Cumming, G.S., Jackson, J.B.C., Kleypas, J., van de Leemput, I.A., Lough, J.M., Morrison, T.H., Palumbi, S.R., van Nes, E.H., Scheffer, M.: Coral reefs in the Anthropocene. Nature, 546, 82-90, http://doi.org/10.1038/nature22901, 2017.

Inoue, M., Suzuki, A., Nohara, M., Hibino, K., Kawahata, H.: Empirical assessment of coral Sr/Ca and Mg/Ca ratios as climate 620 proxies using colonies grown at different temperatures. Geophys. Res. Lett., 34, 1-4, https://doi.org/10.1029/2007GL029628, 2007.

Jiang, Q., Cao, Z., Wang, D., Li, Y., Wu, Z., Ni, J.: Coral Ba/Ca and Mn/Ca ratios as proxies of precipitation and terrestrial input at the eastern offshore area of Hainan Island. J. Ocean Univ. China, 16, 1072–1080, https://doi.org/10.1007/s11802-625 017-3265-0, 2017.

Jochum K.P., Willbold M., Raczek I., Stoll B. and Herwig K.: Chemical characterisation of the USGS reference glasses GSA-1G, GSC-1G, GSD-1G, GSE-1G, BCR-2G, BHVO- 2G and BIR-1G using EPMA, ID-TIMS, ID-ICP-MS and LA- ICP-MS. Geostand. Geoanalytical Res., 29, 285–302, https://doi.org/10.1111/j.1751-908X.2005.tb00901.x, 2005.

630
Jochum, K.P., Stoll, B., Herwig, K., Willbold, M.: Validation of LA-ICP-MS trace element analysis of geological glasses using a new solid-state 193 nm Nd:YAG laser and matrix-matched calibration. J. Anal. At. Spectrom., 22, 112-121, https://doi.org/10.1039/b609547j, 2007.

635 Jochum K.P., Weis U., Stoll B., Kuzmin D., Yang Q., Raczek I., Jacob D.E., Stracke A., Birbaum K., Frick D.A., Guenther D. and Enzweiler J.: Determination of reference values for NIST SRM 610–617 glasses following ISO guidelines. Geostand. Geoanalytical Res., 35, 397–429, https://doi.org/10.1111/j.1751-908X.2011.00120.x, 2011.

JPL MUR MEaSUREs Project: GHRSST Level 4 MUR Global Foundation Sea Surface Temperature Analysis. Ver. 4.1. 640 PO.DAAC, CA, USA, http://doi.org/10.5067/GHGMR-4FJ04, 2015.

Klein, R., Loya, Y.: Skeletal growth and density pattern of two *Porites* corals from the Gulf of Eilat, Red Sea. Mar. Ecol. Prog. Ser., 77, 253-259, http://doi.org/10.3354/meps077253, 1991.

645 Kleypas, J.A., McManus, J.W., Meñez, L.A.B.: Environmental limits to coral reef development: Where do we draw the line? Am. Zool., 39, 146-159, http://doi.org/10.1093/icb/39.1.146, 1999.

Knutson, D.W., Buddemeier, R.W., Smith, S.V.: Coral chronometers: Seasonal growth bands in reef corals. Science, 177, 270-272, http://doi.org/10.1126/science.177.4045.270, 1972.

650
Koop, K., Booth, D., Broadbents, A., Brodie, J., Bucher, D., Capone, D., Coll, J., Dennison, W., Erdmann, M., Harrison, P., Hoegh-Guldberg, O., Hutchings, P., Jones, G.B., Larkum, A.W.D., O'Neil, J., Steven, A., Tentori, E., Ward, S., Williamson, J., Yellowless, D.: ENCORE: The effect of nutrient enrichment on coral reefs. Synthesis of results and conclusions. Mar. Pollut. Bull., 42, 91-120, https://doi.org/10.1016/S0025-326X(00)00181-8, 2001.

655
Lapointe, B.E., Clark, M.W.: Nutrient inputs from the watershed and coastal eutrophication in the Florida Keys. Estuaries, 15, 465-476, https://doi.org/10.2307/1352391, 1992.

Lea, D.W., Shen, G.T., Boyle, E.A.: Coralline barium records temporal variability in equatorial Pacific upwelling. Nature, 660 340, 373-376, https://doi.org/10.1038/340373a0, 1989.

Lee, C.M., Jones, B.H. Brink, K.H., Fischer, A.S.: The upper-ocean response to monsoonal forcing in the Arabian Sea: seasonal and spatial variability. Deep Sea Res. II, 47, 1177-1226, http://doi.org/10.1016/S0967-0645(99)00141-1, 2000.

665 Locarnini, R. A., Mishonov, A. V., Baranova, O. K., Boyer, T. P., Zweng, M. M., Garcia, H. E., Reagan, J. R., Seidov, D., Weathers, K., Paver, C. R., Smolyar, I.: World Ocean Atlas 2018, 1: Temperature, 2018.

Logan, A., Tomascik, T.: Extension growth rates in two coral species from high-latitude reefs of Bermuda. Coral Reefs 63-65, 1991.Lough, J.M., Barnes, D.J.: Environmental controls on growth of the massive coral *Porites*. J. Exp. Mar. Bio. Ecol., 670 245, 225-243, http://doi.org/10.1016/s0022-0981(99)00168-9, 2000.

Lough, J.M., Cantin, N.E., Benthuysen, J.A., Cooper, T.F.: Environmental drivers of growth in massive *Porites* corals over 16 degrees of latitude along Australia's northwest shelf. Limnol. Oceanogr., 61, 684-700, https://doi.org/10.1002/lno.10244, 2016.
675
Manzello, D.P., Enochs, I.C., Bruckner, A., Renaud, P.G., Kolodziej, G., Budd, D.A., Carlton, R., Glynn, P.W.: Galápagos coral reef persistence after ENSO warming across an acidification gradient. Geophys. Res. Lett., 41, 9001-9008, https://doi.org/10.1002/2014GL062501, 2014.

680 Manzello, D.P., Enochs, I.C., Kolodziej, G., Carlton, R.: Recent decade of growth and calcification of *Orbicellla faveolata* in the Florida Keys: an inshore-offshore comparison. Mar. Ecol. Prog. Ser., 521, 81-89, http://doi.org/10.3354/meps11085, 2015.

McCulloch, M.T., D'Olivo, J.P., Falter, J., Holcomb, M., Trotter, J.A.: Coral calcification in a changing world and the 685 interactive dynamics of pH and DIC upregulation. Nat. Commun., 8, 1-8, http://dio.org/10.1038/ncomms15686, 2017.

Mertz-Kraus, R., Brachert, T.C., Jochum, K.P., Reuter, M., Stoll, B.: LA-ICP-MS analyses on coral growth increments reveal heavy winter rain in the Eastern Mediterranean at 9 Ma. Paleogeogr., Paleoclimatol., Paleoecol., 273, 25-40, https://doi.org/10.1016/j.palaeo.2008.11.015, 2009.
690
Mischel, S.A., Mertz-Kraus, R., Jochum, K.P., Scholz, D.: TERMITE: An R script for fast reduction of laser ablation inductively coupled plasma mass spectrometry data and its application to trace element measurements. Rapid Commun. Mass Spectrom., 31, 1079-1087, https://doi.org/10.1002/rcm.7895, 2017.

695 Mollica, N.R., Guo, W., Cohen, A.L., Huang, K., Foster, G.L., Donald, H.K., Solow, A.R.: Ocean acidification affects coral growth by reducing skeletal density. Proceedings of the National Academy of Science of the United States of America, 115, 1754-1759, https://doi.org/10.1073/pnas.1712806115, 2018.

Montaggioni, L.F., Le Cornec, F., Corrège, T., Cabioch, G.: Coral barium/calcium record of mid-Holocene upwelling activity 700 in New Caledonia, South-West Pacific. Palaeogeogr. Palaeoclimatol. Palaeoecol., 237, 436-455, https://doi.org/10.1016/j.palaeo.2005.12.018, 2006.

Montagna, P., McCulloch, M., Douville, E., López Correa, M., Trotter, J., Rodolfo-Metalpa, R., Dissard, D., Ferrier-Pagès, C., Frank, N., Freiwald, A., Godstein, S., Mazzoli, C., Reynaud, S., Rüggeberg, A., Russo, S., Taviani, M.: Li/Mg 705 systematics in scleractinian corals: Calibration of the thermometer. Geochim. Cosmochim. Acta, 132, 288-310, http://doi.org/10.1016/j.gca.2014.02.005, 2014.

Muscatine, L., Porter, J.W.: Reef Corals: Mutualistic Symbioses Adapted to Nutrient-Poor Environments. Bioscience, 27, 454-460, https://doi.org/10.2307/1297526, 1977.
710

Muscatine, L., R. McCloskey, L., E. Marian, R.: Estimating the daily contribution of carbon from zooxanthellae to coral animal respiration. Limnol. Oceanogr., 26, 601-611, https://doi.org/10.4319/lo.1981.26.4.0601, 1981.

Okai, T., Suzuki, A., Kawahata, H., Terashima, S., Imai, N.: Preparation of a new Geological Survey of Japan geochemical reference material: Coral JCp-1. Geostandard Newslett., 26, 95-99, http://doi.org/10.1111/j.1751-908X.2002.tb00627.x, 2002.

Omata, T., Suzuki, A., Sato, T., Minoshima, K., Nomaru, E., Murakami, A., Murayama, S., Kawahata, H., Maruyama, T.: Effects of photosynthetic light dosage on carbon isotope composition in the coral skeleton: Long-term culture of *Porites* spp. J. Geophys. Res., 13, 1-15, https://doi.org/10.1029/2007JG000431, 2008.

Omer, W.M.M.: Ocean acidification in the Arabian Sea and the Red Sea – factors controlling pH. Unpublished master's thesis. University Bergensis, 2010.

Paillard, D., Labeyrie, l., Yiou, P.: Macintosh program performs time-series analysis. Eos Transactions American Geophysical Union, 77, 379, https://doi.org/10.1029/96EO00259, 1996.

Perry, C.T., Edinger, E.N., Kench, P.S., Murphy, G.N., Smithers, S.G., Steneck, R.S., Mumby, P.J.: Estimating rates of biologically driven coral reef framework production and erosion: A new census-based carbonate budget methodology and applications to the reefs of Bonaire. Coral Reefs, 31, 853-868, https://doi.org/10.1007/s00338-012-0901-4, 2012.

Quinn, N.J., Johnson, D.W.: Cold water upwellings cover Gulf of Oman coral reefs. Coral Reefs, 15, 214, 1996.

Risk, M.J., Sammarco, P.W.: Cross-shelf trends in skeletal density of the massive coral *Porites lobata* from the Great Barrier Reef. Mar. Ecol. Prog. Ser., 69, 195-200, http://doi.org/10.3354/meps069195, 1991.

Ross, C.L., DeCarlo, T.M., McCulloch, M.T.: Environmental and physiological controls on coral calcification along a latitudinal temperature gradient in Western Australia. Glob. Change Biol., 25, 431-447, https://doi.org/10.1111/gcb.14488, 2019a.

Ross, C.L., DeCarlo, T.M., McCulloch, M.T.: Calibration of Sr/Ca, Li/Mg and Sr-U paleothermometry in branching and foliose corals. Paleoceanogr. Paleoclimatol., 34, 1271-1291, https://doi.org/10.1029/2018PA003426, 2019b.

Salm, R.V.: Coral reefs of the Sultanate of Oman. Atoll Res. Bull., 380, 1-85, http://doi.org/10.5479/si.00775630.380.1, 1993.

Scoffin, T.P., Tudhope, A.W., Brown, B.E., Chensang, H., Cheeney, R.F.: Patterns and possible environmental controls of skeletogenesis of *Porites lutea*, South Thailand. Coral Reefs, 11, 1-11, https://doi.org/https://doi.org/10.1007/BF00291929, 1992.

Smith, R. L., Bottero, J.S.: On upwelling in the Arabian Sea, In: Angel, M., A Voyage of Discovery. Pergamon, Tarrytown, N.Y.,70th Anniversary Volume, 291-304, 1977.

Smith, S.L.: Understanding the Arabian Sea: Reflections on the 1994-1996 Arabian Sea expedition. Deep Sea Res. II, 48, 1385-1402, https://doi.org/10.1016/S0967-0645(00)00144-2, 2001.

Sun, D., Su, R., McConnaughey, T.A., Bloemendal, J.: Variability of skeletal growth and $\delta^{13}C$ in massive corals from the South China Sea: Effects of photosynthesis, respiration and human activities. Chem. Geol., 255, 414-425, https://doi.org/10.1016/j.chemgeo.2008.07.012, 2008.

760 Swallow, J.C., Bruce, J.G.: Current measurements off the Somali coast during the southwest monsoon of 1964. Deep Sea Res., 13, 861-888, https://doi.org/10.1016/0011-7471(76)90908-6, 1966.

Takahashi, T., Sutherland, S.C., Chipman, D.W., Goddard, J.G., Ho, C.: Climatological distributions of pH, pCO_2, total CO_2, alkalinity, and $CaCO_3$ saturation in the global surface ocean, and temporal changes at selected locations. Mar. Chem.,
765 164, 95-125, https://doi.org/10.1016/j.marchem.2014.06.004, 2014.

Tanaka, K., Holcomb, M., Takahashi, A., Kurihara, H., Asami, R., Shinjo, R., Sowa, K., Rankenburg, K., Watanabe, T., McCulloch, M.: Response of *Acropora digitifera* to ocean acidification: constrains from $\delta^{11}B$, Sr, Mg, and Ba composition of aragonitic skeletons cultured under variable seawater pH. Coral Reefs, 34, 1139-1149,
770 https://doi.org/10.1007/s00338-015-1319-6, 2015.

Tomascik, T., Sander, F.: Effects of eutrophication on reef-building corals. Mar. Biol., 87, 143-155, https://doi.org/10.1016/0198-0254(87)90298-6, 1985.

775 Tomascik, T.: Growth rates of two morphotypes of *Montastrea annularis* along a eutrophication gradient, Barbados, W.I. Mar. Pollut. Bull., 21, 376-381, https://doi.org/10.1016/0025-326X(90)90645-O, 1990.

Tudhope, A.W., Lea, D.W., Shimmield, G.B., Chilcott, C.P., Head, S.: Monsoon climate and Arabian Sea coastal upwelling recorded in massive corals from southern Oman. Palaios, 11, 347-361, https://doi.org/10.2307/3515245, 1996.
780
Vermeij, M.J.A., van Moorselaar, I., Engelhard, S., Hörnlein, C., Vonk, S.M., Visser, P.M.: The effect of nutrient enrichment and herbivore abundance on the ability of turf algae to overgrow coral in the Caribbean. PLoS One, 5, 1-8, https://doi.org/10.1371/journal.pone.0014312, 2010.

785 Wellington, G.M., Glynn, P.W.: Environmental influences on skeletal banding in Eastern Pacific (Panama) corals. Coral reefs, 1, 215-222, http://doi.org/10.1007/BF00304418, 1983.

Wilson, S.: Ecology of coral communities in a marginal environment: Southern Arabia. Unpublished doctoral thesis. University of Warwick, http://doi.org/10.13140/RG.2.2.26085.40164, 2007.
790
Wizemann, A., Nandini, S.D., Stuhldreier, I., Sánchez-Noguera, C., Wisshak, M., Westphal, H., Rixen, T., Wild, C., Reymond, C.E.: Rapid bioerosion in a tropical upwelling coral reef. PLoS One, 13, 1-22, https://doi.org/10.1371/journal.pone.0202887, 2018.

795 Zinke, J., D'Olivo, J.P., Gey, C.J., McCulloch, M.T., Bruggemann, J.H., Lough, J.M., Guillaume, M.M.M.: Multi-trace-element sea surface temperature coral reconstruction for the southern Mozambique Channel reveals teleconnections with the tropical Atlantic. Biogeoscience, 6, 695-712, https://doi.org/10.5194/bg-16-695-2019, 2019.